



The Status of the Design of the PHIN Spectrometer Line Diagnostics for Time Resolved Energy Measurements and First Results from 2009

D. Egger^{1,2}, A. Dabrowski², and T. Lefèvre²

¹*Ecole Polytechnique Federale de Lausanne, CH-1015, Lausanne, Switzerland*

²*CERN, CH-1211 Geneva 23, Switzerland*

Abstract

Within the framework of the second Joint Research Activity PHIN of the European CARE program, a new photo-injector, for proposed use for the CTF3 drive beam, has been designed and installed by a collaboration between LAL, CCLRC and CERN. The PHIN photo-injector is currently being commissioned at CERN. This note addresses the design of the beam diagnostics installed in PHIN, used to measure the energy and energy spread of the beam, which is required to have less than one percent variation along the 1.2 μ s pulse train. The spectrometer line consists of a 90° dipole bending magnet, an Optical Transition Radiation (OTR) screen, coupled to an intensified gated camera for a precise transverse profile measurement and a segmented dump for a time resolved energy measurement. The design of the instruments and some recent commissioning measurements with beam will be presented. Finally improvements for the next commissioning run will be discussed.

Geneva, Switzerland

February 1, 2010

Contents

1	Introduction to the PHIN Spectrometer line	2
2	The OTR screen	3
3	Design of a Segmented Dump for PHIN beam parameters	4
4	Measurements with beam	7
4.1	Comparisons of the beam profile measured with the Segmented Dump and with the Screen	8
4.2	Degradation of the OTR screen surface	9
4.3	Segmented dump Measurements	10
4.3.1	Beam Loading Compensation	11
4.3.2	RF power correlation	13
5	Conclusion and Future Improvements	14
6	Acknowledgments	15
A	Appendix	16

1 Introduction to the PHIN Spectrometer line

The PHIN photo-injector produces a $1.2 \mu\text{s}$ pulse bunched at 1.5 GHz. The nominal beam parameters include: mean energy: $E_0 = 5.6 \text{ MeV}$, energy spread: $\Delta E/E_0 \leq 1\%$ and bunch charge: $q_b = 2.3 \text{ nC}$ [1]. Furthermore it must be ensured that the time resolved mean energy and energy spread are constant. Since the bunch train is long and the acceleration fully loaded, it is expected to have heavy beam loading. Therefore it is necessary to design a time resolved spectrometer capable of measuring mean energy and a relative energy spread with a resolution below 1%, and checking that the gun is operated in the compensated beam loading regime [2].

The PHIN spectrometer line consists of: A 90° dipole bending magnet; a screen emitting Optical Transmission Radiation (OTR) as the beam passes through it [3]; an intensified camera for a precise transverse profile measurement using the OTR light; and a segmented dump for a time resolved energy measurement, as shown schematically in Figure 1. The present diagnostics in the spectrometer line evolved from an early setup [4], used before the summer of 2009, in order to be better adapted to measure the time resolved energy and the energy spread of the beam. The current setup, summarized in Table 1, will be described in more detail in the Section 2 and in Section 3 with recent measurements to understand the performance of the diagnostics with beam will be discussed in Section 4. Finally, in Section 5 we suggest some improvements to the instrumentation setup to be considered before the next PHIN run in 2010.

Diagnostic	Distance from Dipole Magnet	Material	Geometry
OTR Screen with Intensified Gated Camera	58.0 cm	25 μm thick aluminized mylar foil ellipse (158 mm x, 56 mm y)	fixed support tilted 45°
Segmented Dump	75.5 cm	stainless steel segments Epoxy resin insulators	20, 2 mm segments 20, 1 mm spacers

Table 1: Summary of the PHIN Spectrometer diagnostics

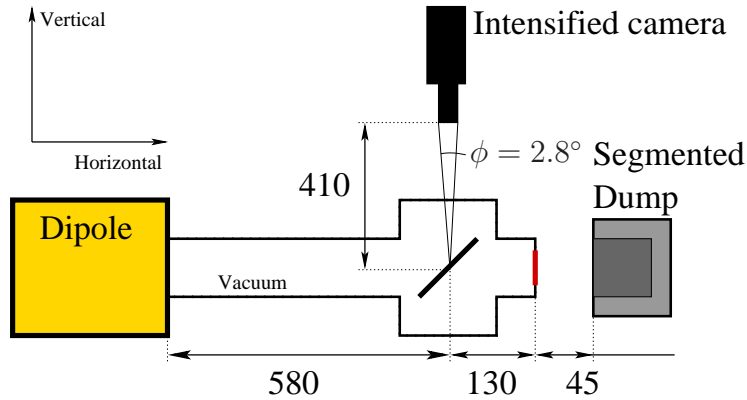


Figure 1: Layout of the PHIN spectrometer line. Dimensions are in mm.

2 The OTR screen

Prior to summer 2009, for the early commissioning of PHIN at low energy and low bunch charge, a fixed alumina phosphorescence screen was installed in the beam line [4], located at 58.0 cm from the exit of the dipole magnet. However, it was removed because at an electron beam energy of 5.5 MeV, the screen absorbed about 16.5% of the beam energy and in addition, scattering inside the alumina increased the exiting beam's divergence. This effect introduced a relative error in the energy spread measurement with the segmented dump of 290% [5], making it unusable.

Geant4 [6] simulations, shown in Figures 3(a) and 3(b), compare the effect of the previous alumina screen with the OTR screen installed in the Fall of 2009. The now installed non-movable OTR screen broadens the beam distribution by 14 mrad corresponding to a 17.9% increase of the transverse beam size by the time it reaches the vacuum window. Thus, after correcting for this effect, which will be discussed in more detail in Section 3, a time resolved measurement with the segmented dump, at the end of the line, is still achievable.

The new OTR screen, is a 25 μm thick aluminized mylar foil tilted at 45° with respect to the beam, see Figure 1. By passing through this screen the electron beam produces OTR which is imaged by a Proxitronic NANOCAM HF4 V 5N intensified camera, sensitivity in the 200 – 600 nm range, see Appendix A . The objective, with a 50 mm focal length, is located at 410 mm from the center of the OTR screen and has an opening angle of $\phi = 2.8^\circ$, see Figure 1. The maximum of the OTR light distribution is found at an emission angle of 4.8°, see Figure 2(a). With an energy spread of 1% at 1σ , the transverse acceptance of the 158 mm wide screen corresponds to 27 times the design size due to beam divergence caused

by the dipole. The resolution of the image is $185 \mu\text{m}/\text{pixel}$ in the horizontal direction.

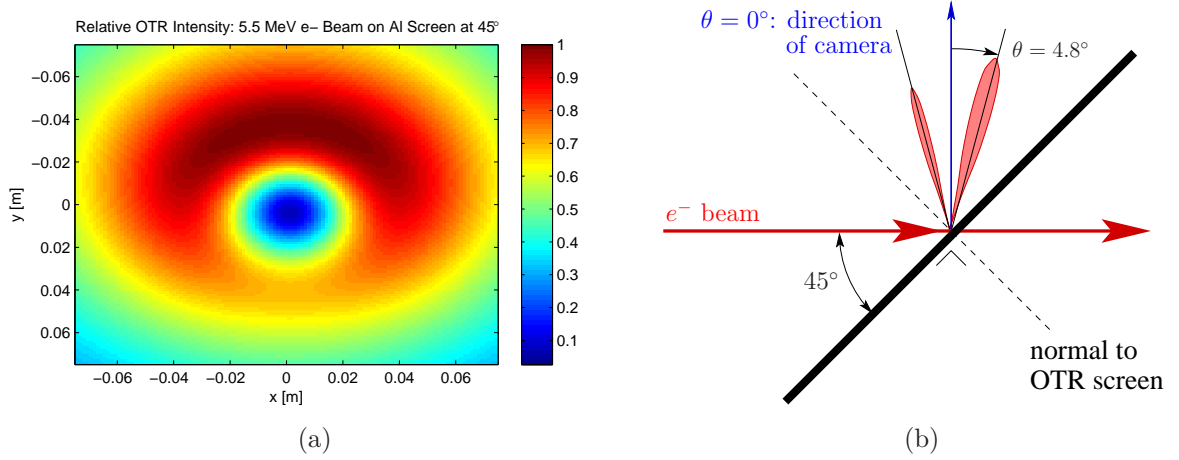


Figure 2: (a) The relative photon intensity distribution, produced by a 5.5 MeV electron beam on a Al screen tilted at 45° , in the plane perpendicular to the entrance of the camera. (b) Schematic of the OTR screen geometry featuring the OTR lobes of interest.

3 Design of a Segmented Dump for PHIN beam parameters

The time resolved energy spread of the beam is measured using a device called a ‘‘Segmented Dump’’ installed at the end of the spectrometer line. It is composed of parallel metallic plates, segmented in x , in which the beam is stopped and thus create a current, proportional to the incoming transverse beam intensity. An additional collimator can be used to improve the resolution of the measurements, for special cases when the incoming beam has a low divergence, at the cost of signal to noise ratio. For the subsequent measurements presented here the collimator was not used. The optimal transverse segmentation, and the choice of materials to be used, depends on the nominal beam parameters given previously in Section 1.

The material used for the segmented dump was chosen using Geant4 simulations. Five different materials were simulated, the one capable of withstanding the thermal load and producing the less backscattering is used. Table 4(a) shows that iron based materials are good candidates. Therefore stainless steel (grade 304L) was chosen since it is inexpensive and the temperature increase was found to be negligible, see Figure 4(b).

Based on PARMELA simulations, the expected 1σ horizontal transverse size of the beam and the beam envelope, i.e. σ_{beam} , at the dump are shown in Table 2 [7]. These quantities are defined by: $\sigma_x^2 = \langle x^2 \rangle - \langle x \rangle^2$ and $\sigma_{beam}^2 = \langle x_\beta^2 \rangle - \langle x_\beta \rangle^2$ where the position of the particles is given by: $x(s) = x_\beta(s) + D(s)\delta$. Geant4 simulations showed that σ_x is broadened by 79%, due to the vacuum window and the fixed OTR screen in front of the dump, see Figure 5(a). Thus, for a single shot measurement the width of the dump was chosen to be 6 cm, corresponding to more than 7 time the optimal transverse size. At PHIN energies, the broadening due to multiple scattering inside the dump is negligible. Hence the minimum segment width was chosen to be 5 times the rms of the broadening of a pencil beam due to all the physics processes, i.e. the segments need to be thicker than 1 mm. Based on the considerations in

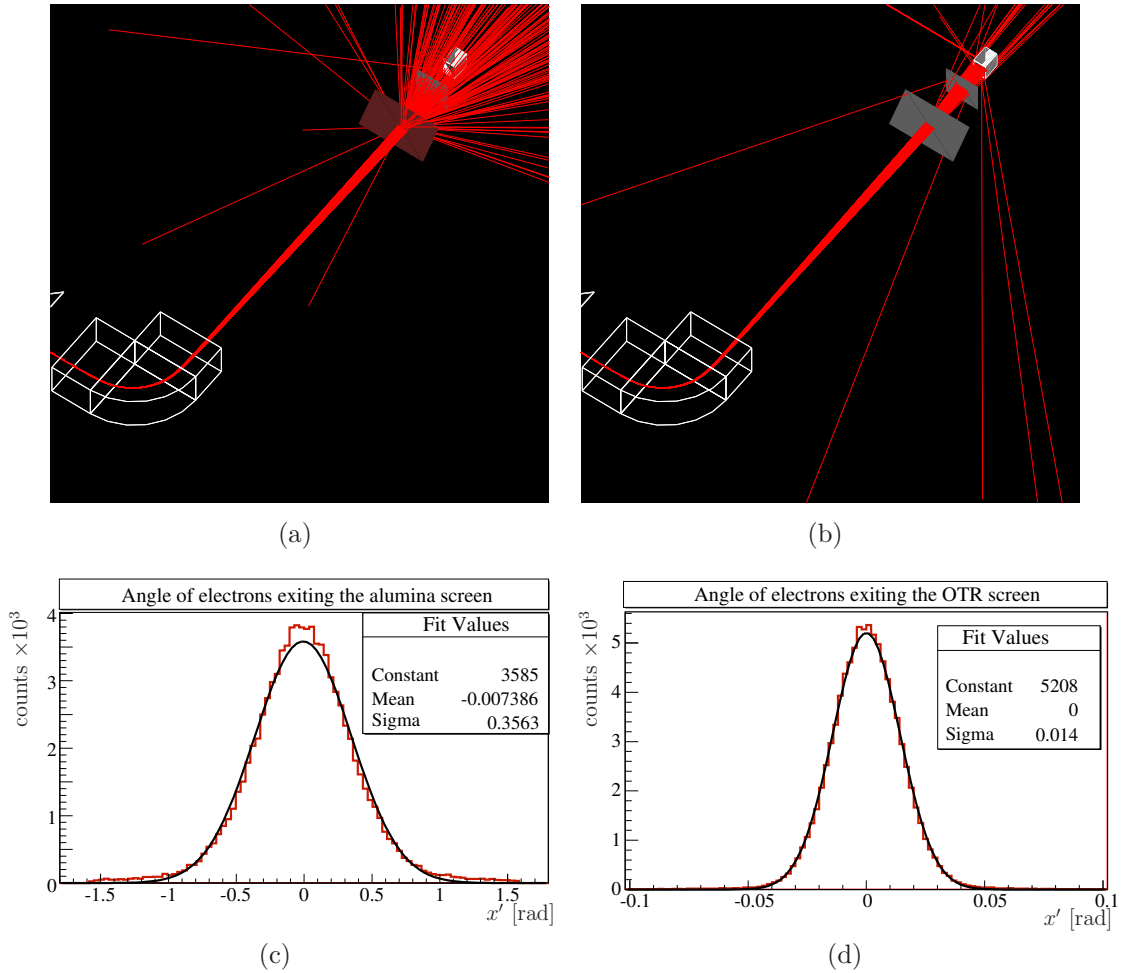


Figure 3: (a) Geant4 simulation of the beam line featuring the Alumina phosphorescence screen. (b) Geant4 simulation featuring the OTR screen. (c) and (d) Angle of a pencil beam exiting the Alumina and OTR screens respectively.

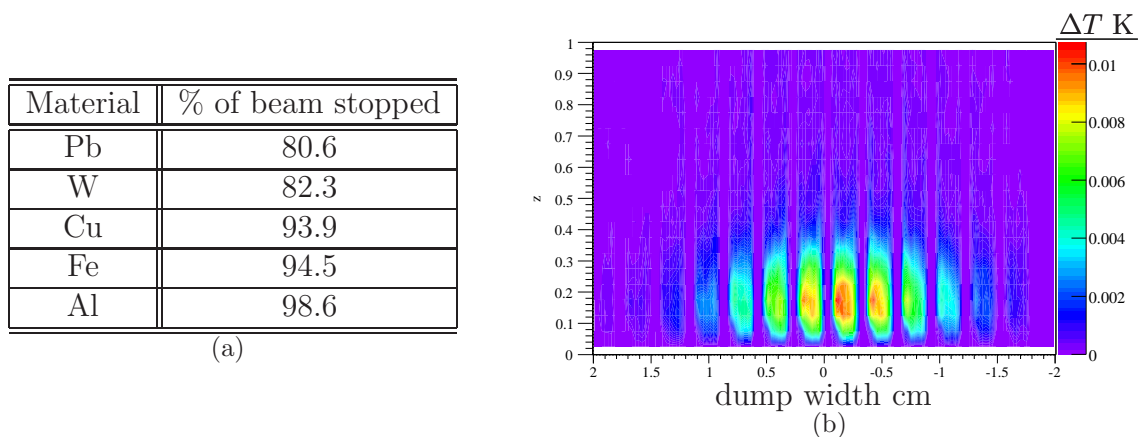


Figure 4: (a) Fraction of beam stopped by different materials. (b) Thermal load on the dump made of stainless steel 304L for a nominal PHIN pulse. The maximum temperature increase in a volume element of size $dV = 738 \mu\text{m}^3$ is $\Delta T = 11 \text{ mK}$.

[8], the dump features 20 channels for a segment density of 4 segments/ σ , their thickness was chosen to be 2 mm, giving an error of 0.35% for a relative energy spread of 1%. The dump is 5 cm deep corresponding to 10.8 times the CSDA¹ range of 5.5 MeV electrons in iron. Thus the dump stops more than 99.9% of the electrons that do not backscatter.

Solenoid 1 current	Solenoid 2 current	transverse size σ_x	beam envelope: σ_{beam}
[A]	[A]	[mm]	[mm]
200	200	9.03	0.68
200	210	7.79	0.71
200	220	8.31	0.93

Table 2: Transverse size of beam on the dump for different solenoid settings without the elements in the beam line.

The segments are held in place by an anticordal² frame onto which the collimator or a frame can be screwed, see Figure 6(b). Epoxy resin was chosen as the insulator and is shielded from the beam by the frame, thus protecting it from some radiation, see Figure 6(a). The amount of time between the creation of an ideal beam at 1.05 m downstream of the segmented dump, and when the individual electrons are stopped in the dump, is shown in Figure 5(b), as simulated using Geant4. From this figure, the intrinsic time resolution due to the physics processes in the dump, is estimated to be about 17 ps. The current from the dump is read out over 50 Ω resistors and connected via lemo-to-BNC connectors to type CB50 cables of 55 m in length to ADCs in the klystron gallery (building 2001 RA-38) sampling at 96.1 MHz. This makes the electronics the limit for the bandwidth in this present configuration, although it could be modified in the future if improved time resolution was required. The crosstalk between channels below 100 MHz was measured to be 10 dB.

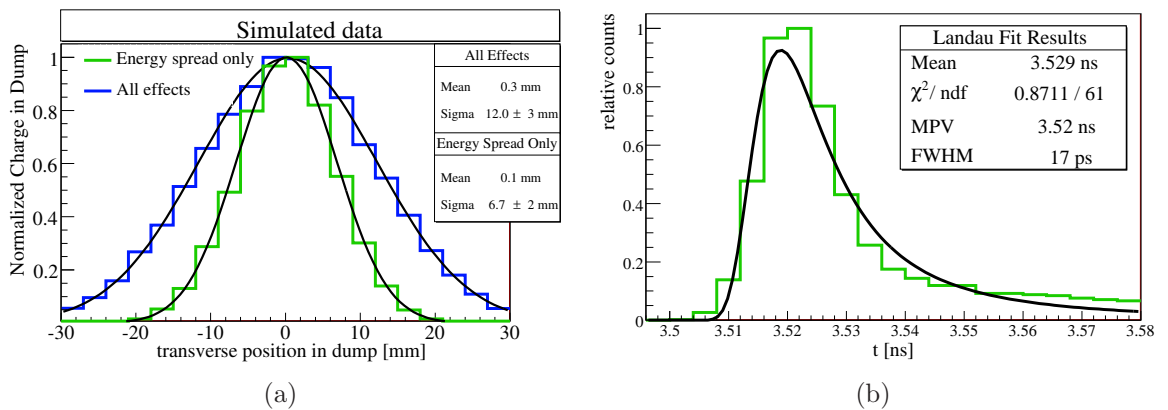


Figure 5: (a) The simulated transverse beam profile at the position of the dump, estimating the broadening of the beam due to the elements (incl. the OTR screen and vacuum window) in the spectrometer beam line. (b) Time at which the electrons lose all their kinetic energy in the segmented dump, fit to a Landau distribution.

¹Approximation of the mean path length of charge particles traveling in matter

²Mg: 0.6%, Si: 0.4-1.4%, Al: ~97%

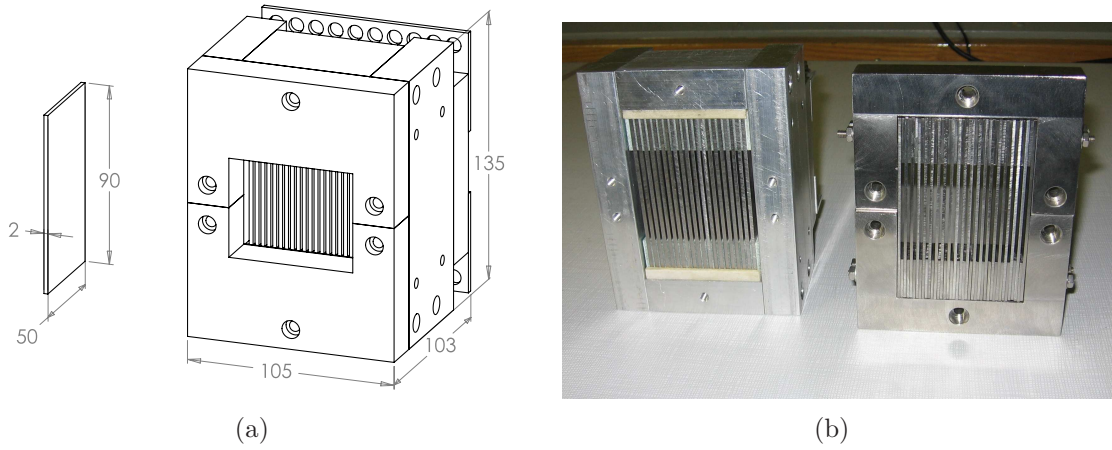


Figure 6: (a) Mechanical drawing of the segmented dump (in mm); Left: one segment. (b) Photograph of the assembled dump (left) and the collimator (right)

4 Measurements with beam

The data presented here was taken during the PHIN run in September 2009. The energy spread is obtained in the following way: Both instruments rely on the fact that the dipole deflects particles of different energies according to:

$$p = \frac{q}{\alpha} \int B dl \quad (1)$$

Thus the dispersion function at the OTR screen and the dump is $D_{OTR} = 820.2$ mm and $D_{dump} = 1067.7$ mm respectively.

The pictures taken by the intensified camera yield the horizontal and vertical transverse profile of the beam, see Figure 8(a). Projecting this data onto the horizontal plane, shown in 8(b), gives a profile that encodes the time integrated energy spread which is then fit to a Gaussian distribution.

In the segmented dump, the time resolved energy of the beam is reconstructed using the current produced in the 20 channels to obtain a 2D contour plot, for example, see Figure 8(c). The current, sliced in time and as function of segment position is then fit to a Gaussian distribution yielding the time resolved energy of the beam.

PARMELA simulations allow a calculation of the expected transverse beam dynamics contribution to the horizontal profile [4]. This results in a correction term of σ_{beam} for both devices. In the case of the segmented dump, Geant4 simulations show that the beam acquires an additional Gaussian divergence σ'_s after the OTR screen and must drift over a distance $L_1 = 130$ mm to the vacuum window, broadening the transverse profile. The same is true for the effect of the vacuum window, with an additional divergence σ'_{vac} and a drift of distance L_2 to the dump. These effects need to be accounted for, to extract a meaningful energy spread. Therefore, the measured profile at the dump and the OTR screen, σ_{dump} and σ_{OTR} respectively, are corrected in the following manner:

$$\sigma_{E,dump} = \sqrt{(\sigma_{dump} - L_1 \tan(\sigma'_s) - L_2 \tan(\sigma'_{vac}))^2 - \sigma_{beam}^2} \quad (2)$$

$$\sigma_{E,OTR} = \sqrt{\sigma_{OTR}^2 - \sigma_{beam}^2} \quad (3)$$

The contribution from the OTR screen, σ'_s , could be removed by installing the screen on a movable support. This was not considered for the moment, due to the costs involved in modifying the vacuum assembly and associated mechanics. The uncorrected data, corresponding to σ_{dump} , is shown as an example in Figure 8(d) as the black Gaussian, and the corrected fit, i.e. $\sigma_{E,dump}$ is shown in green.

For both instruments, the energy on the x axis corresponds to the horizontal position. Assuming that the center of the segmented dump and the screen lie at a 90° deflection angle, then the calibration between central momentum and magnet current is given by [9]: $p_{center} = 0.52I_{dipole}$. Finally, to first order, equation (1) gives the relation between the position x (in mm) and the momentum (in MeV/c). For the segmented dump and the screen, the calibrations are:

$$Dump : p(x) = 0.52I_{dipole} \left(1 + \frac{x}{755}\right) \quad (4)$$

$$OTR : p(x) = 0.52I_{dipole} \left(1 + \frac{x}{580}\right) \quad (5)$$

Figure 7 shows the raw signals inside the segmented dump for a typical $1.2 \mu s$ pulse. The rise time was found to be less than 20 ns confirming that the electronics are the limiting factor for time resolution, in the present configuration.

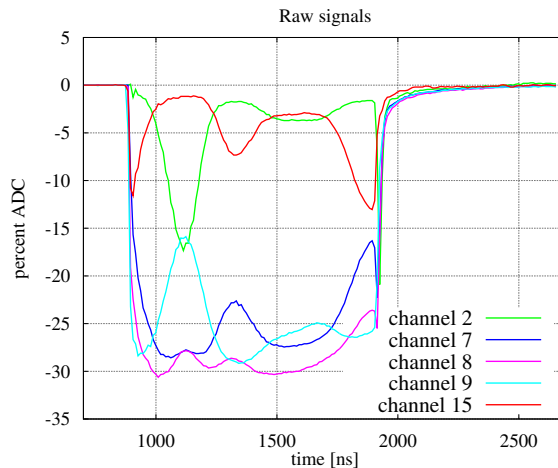


Figure 7: Raw signals measured by the dump, where the lowest energy corresponds to the lower channel numbers, increasing to higher energy with higher channel number.

4.1 Comparisons of the beam profile measured with the Segmented Dump and with the Screen

The average energy spread measured by the screen can be compared to the segmented dump in the following way: Integrating the current from the dump with respect to time yields the total charge in the dump, see Figure 8(d). This is equivalent to the projection from the OTR i.e. Figure 8(b). From the mean of the resulting distribution, x_0 , we define E_0 using relations (4) and (5). Then the energy at 1σ , i.e. $E_{1\sigma}$, is given by the same relations but using $x = x_0 + \sigma_E$ where σ_E is the standard deviation of the Gaussian fit.

The result is summarized in Table 3. It can be seen that the corrected transverse size, σ_E of the dump agrees better with the expected values from simulation σ_{sim} than the OTR

screen. Simulations also indicate that the agreement between the dump and OTR screen should be better than 12% and within the fitting errors. Experiments show that the OTR screen and the segmented dump agree within 25%. In the future this can be improved; The mean energy measured by the screen and the segmented dump differ by a few mm suggesting a misalignment between these two devices, which will be measured with beam in the next run, and corrected. Furthermore, it was found that the OTR screen was damaged during the run and will be discussed further in Section 4.2, making its results less trustworthy than those of the segmented dump.

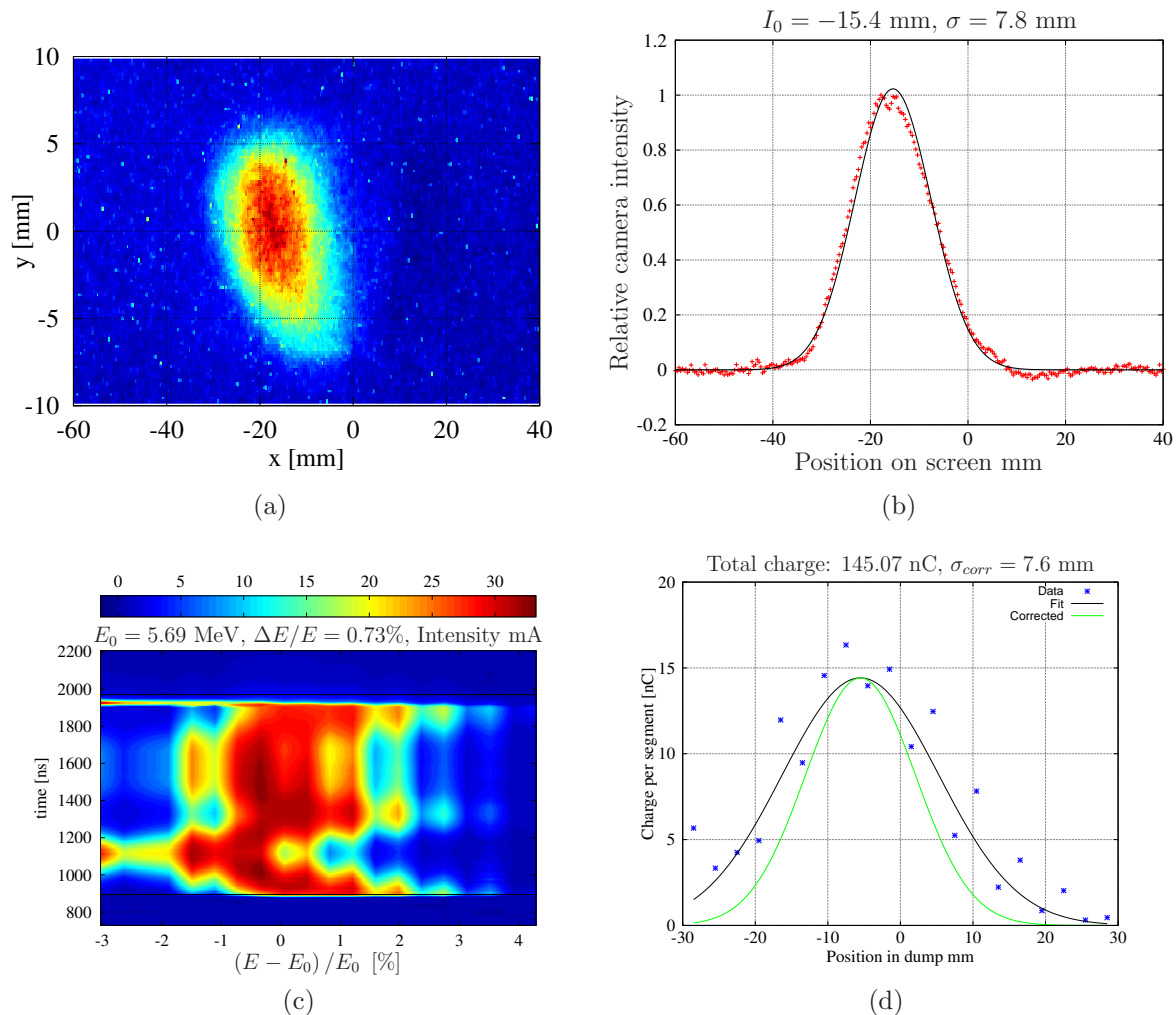


Figure 8: (a) Image of the beam taken by the intensified camera. (b) Projection of the image onto the horizontal plan. (c) Time resolved energy spectrum in the segmented dump. (d) Time integrated current. The profile has been fitted to a Gaussian distribution (black) and then corrected for the effect of the elements in the beam line (green).

4.2 Degradation of the OTR screen surface

The exact mechanism for the degradation of the screen surface over time is not fully understood yet, however both from inspection of the screen surface after the Fall 2009 PHIN run and from beam based measurements, the damage is visible, see Figure 9(a).

	σ_E [mm]	σ_{sim} [mm]	E_0 [MeV]	$E_{1\sigma}$ [MeV]	σ [keV]	$\Delta E/E$ %
OTR	7.8 ± 0.01	5.5	5.625 ± 0.001	5.673 ± 0.001	48 ± 1	0.85 ± 0.02
Dump	7.6 ± 0.9	7.2	5.693 ± 0.005	5.735 ± 0.005	42 ± 5	0.73 ± 0.02

Table 3: Comparison between OTR and the segmented dump results. The two instruments agree within 25%.

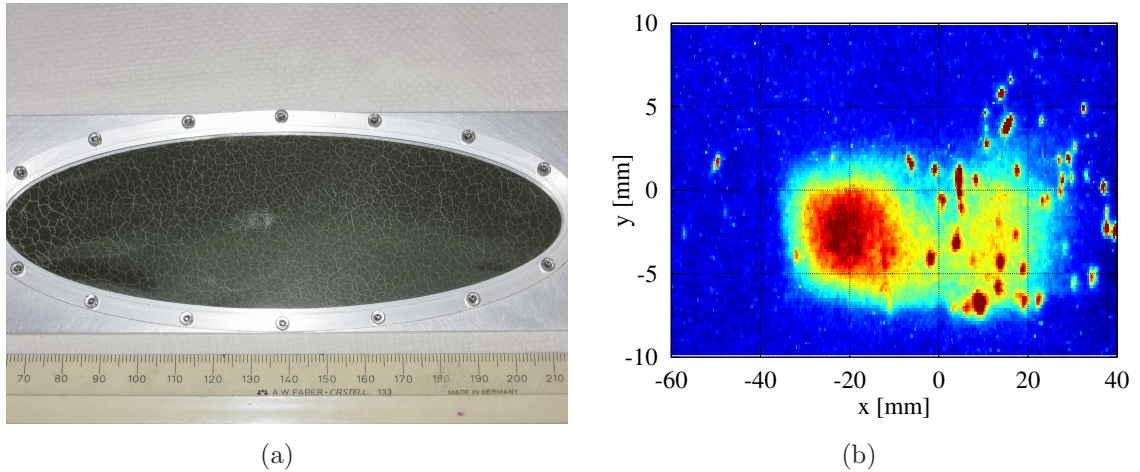


Figure 9: (a) A photograph of the aluminized mylar spectrometer screen after the 3 week PHIN run, showing surface damage. (b) Image using the spectrometer OTR screen, during a beam measurement, showing some non-uniform behavior on the screen surface.

During some beam based measurements of the beam profile, some non-uniform radiation is imaged, see Figure 9(b). The profile measured in this particular image is unusual, indicating that the screen seems to have lost some reflectivity in the central region. This screen damage, in addition due to the large opening angle of the OTR lobe at a beam energy of 5.5 MeV, see Figure 2(a), compared with the numerical acceptance of 2.8 degrees, has resulted in a reduced light collection in the central region of the screen.

This damage might be a result of the high surface currents flowing through the several nanometer thin layer of aluminum deposited on the mylar substrate. The intensified camera is most sensitive in the optical and near ultraviolet (UV) wavelengths, see Figure 15. The beam image in Figure 9(b) might also have a UV contribution, corresponding to the intense bright spots on the image. These appear to be local sparks rather than beam islands.

Therefore, this damage to the OTR screen, and the present configuration of the optical line, makes transverse profile measurements in this configuration for the 2009 Fall measurements unreliable.

4.3 Segmented dump Measurements

PHIN's main objective is to produce a long pulse with a high bunch charge and very good time stability in energy and energy spread. In what follows, is shown how the segmented dump was used as an essential diagnostic tool in identifying the source of energy fluctuations in the pulse, and thus allowing for immediate, inline feedback to achieve stable, time resolved

beam energy conditions.

4.3.1 Beam Loading Compensation

In PHIN, the beam loading is compensated by changing the timing between the RF and the laser producing the beam. Measurements with the segmented dump can be used to monitor the resulting energy spread along the pulse, depending on the amount of beam loading compensation. In Figure 10(a), the current in the dump as function of the beam energy and time, for an under compensated beam, is shown; as shown in Figure 10(b), the RF power in the cavity is stronger at the beginning of the pulse, giving the head of the beam more energy. In Figure 11, this effect has been over compensated; the beam enters the gun before the RF has had enough time to fill the entire cavity. The resulting beam has now a low energy head. When the timing is chosen correctly and for the same beam parameters, the produced beam has less energy variations along the pulse train and the RF power during the pulse is close to constant as shown in Figures 12 and 13. This also produces a beam with a smaller energy spread.

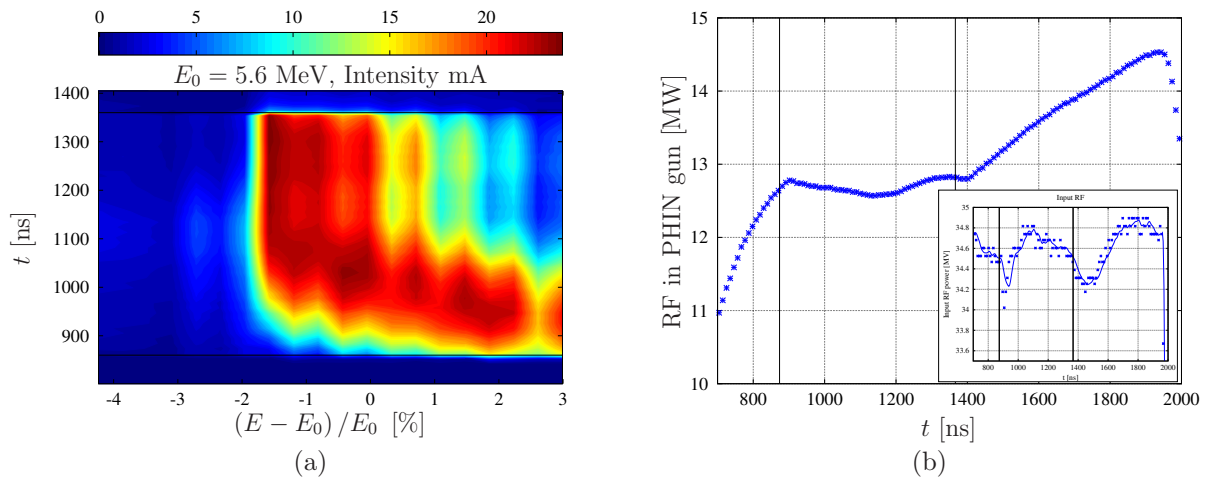


Figure 10: Case where beam loading is under compensated. (a) Segmented dump spectrum. (b) RF power in PHIN gun and input power.

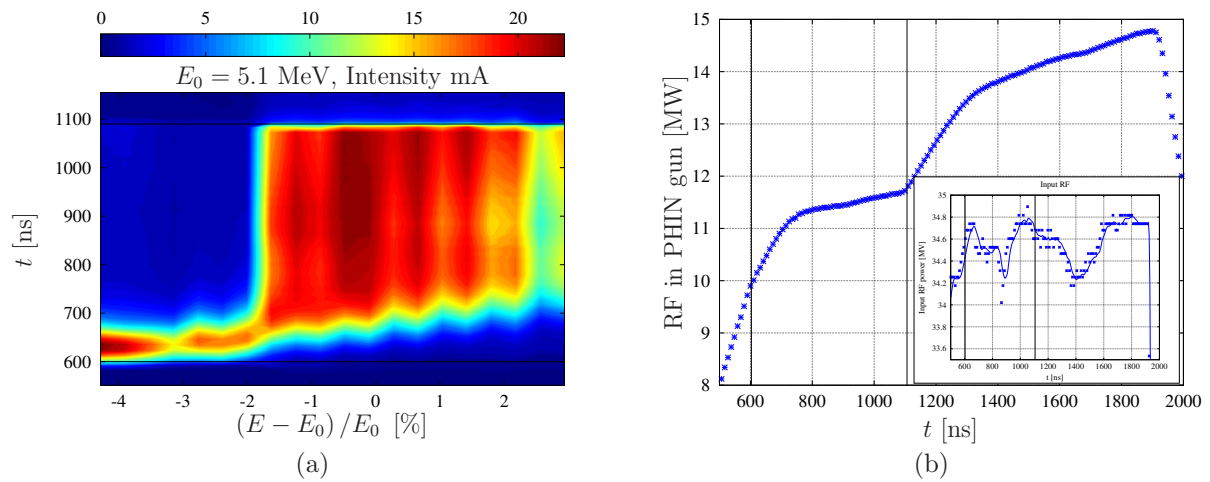


Figure 11: Case where beam loading is over compensated. (a) Segmented dump spectrum. (b) RF power in PHIN gun and input power.

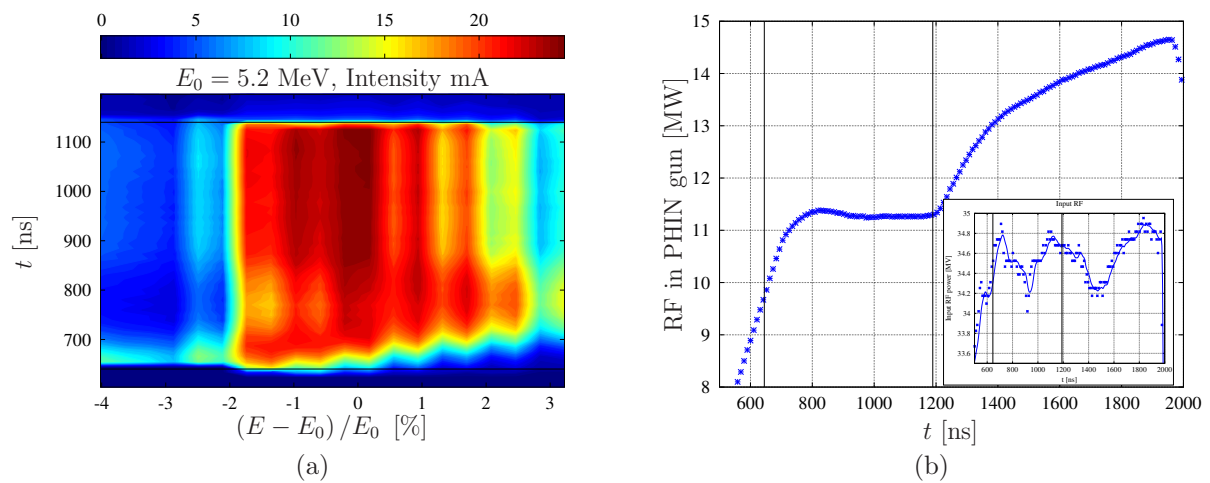


Figure 12: Case where beam loading is well compensated. (a) Segmented dump spectrum. (b) RF power in PHIN gun and input power.

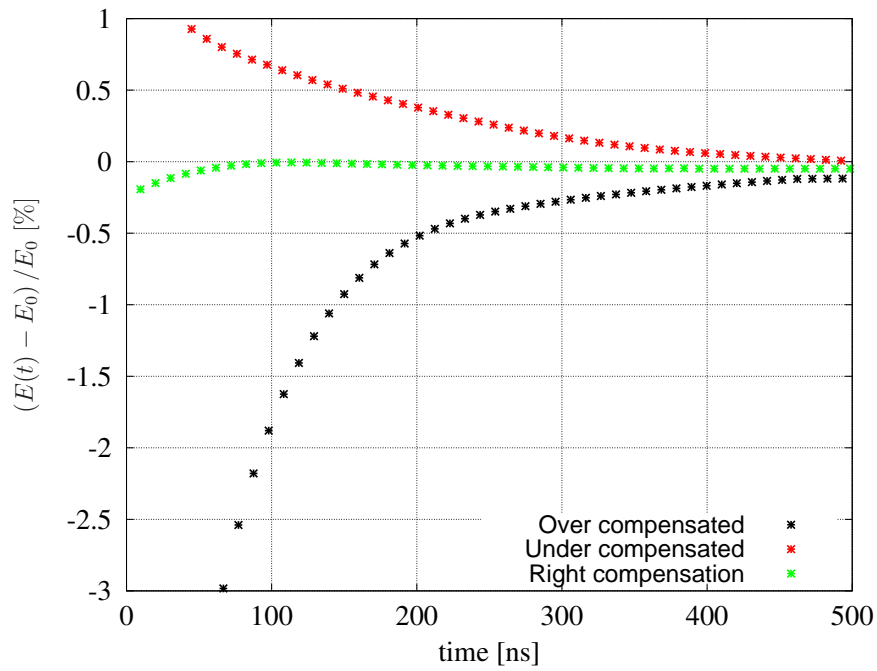


Figure 13: Relative mean time resolved energy fluctuations for all three cases.

4.3.2 RF power correlation

The segmented dump can be used to identify energy variations in the beam due to the RF. The fluctuations in Figure 14(a) can be traced back to the RF power variations along the pulse train shown in Figure 14(b). The strong correlation between the RF as seen by the gun, and the energy as measured with the segmented dump is shown in Figure 14(c). Fluctuations of the time resolved mean energy, $(E(t) - E_0) / E_0$, displayed in blue in Figure 14(d), indicate that it is the amplitude of the RF power (Figure 14(b)) that is responsible for the variations.

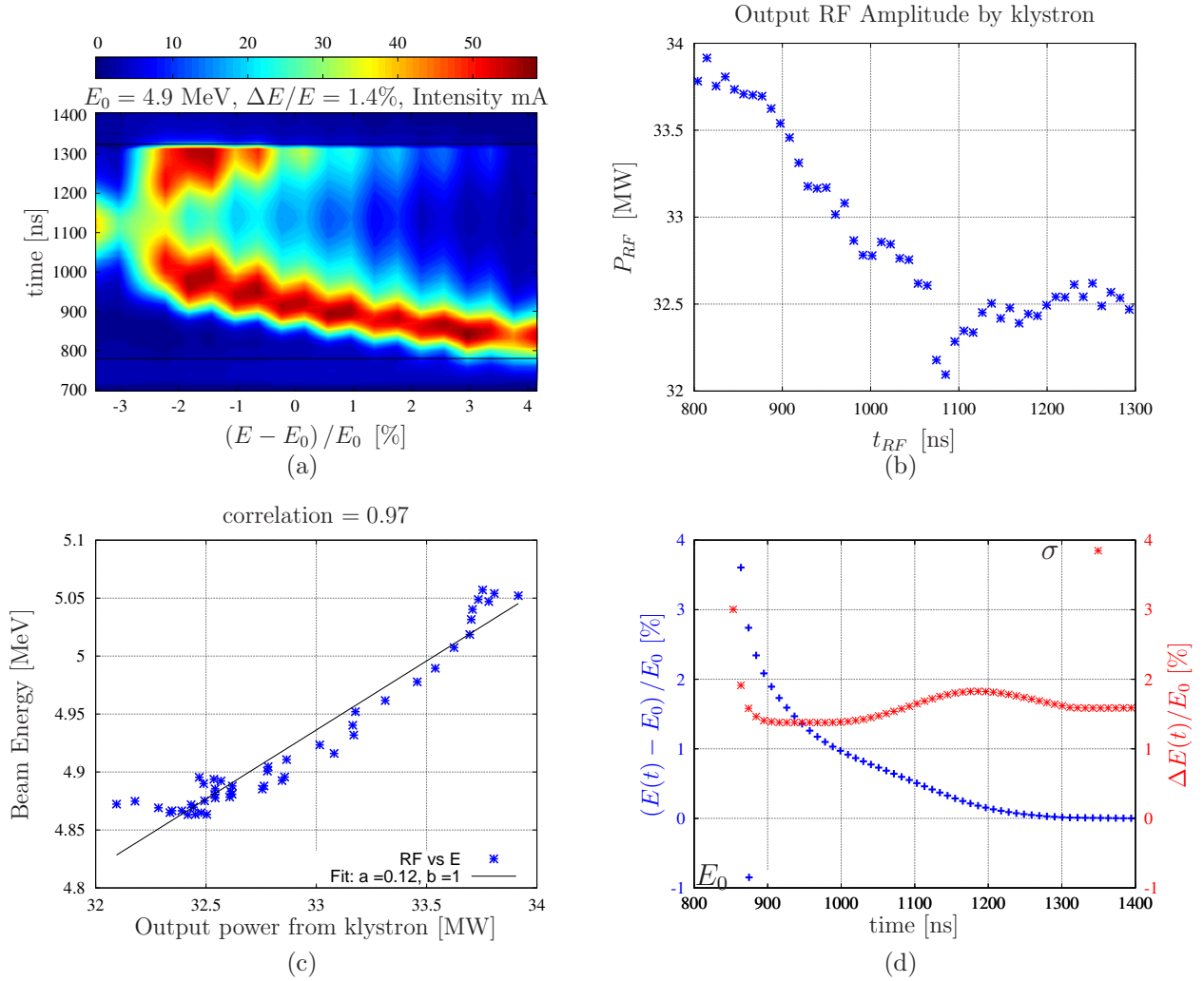


Figure 14: (a) Variation of the beam energy along the pulse train due to RF power instability. (b) Fluctuations in the RF power amplitude. (c) Beam energy as function of the RF power. (d) Time resolved mean energy and energy spread normalized to the central time integrated energy.

5 Conclusion and Future Improvements

The segmented dump presented here has been successfully designed to measure the energy variations along the beam pulse. It can be used to measure the optimal RF settings for beam loading compensation and to identify fluctuations of the RF in amplitude and phase along the pulse.

Future improvements to the spectrometer line diagnostics will be focused on modifying the damaged OTR screen and the corresponding optical line, to improve the transverse beam profile resolution as measured with the OTR screen and intensified camera. Since the emission angle of the OTR lobes at a beam energy of 5.5 MeV, is rather large (4.8°) and the intensity of the two lobes is asymmetric, it is recommended that either the OTR screen, be re-aligned in the MTV tank to an angle of $(45 + 4.8)^\circ$ with respect to the beam axis, or alternately, that the camera be tilted at angle of 4.8° and displaced in x, in order to capture the central part of the second OTR lobe, yielding about a factor of X10 higher light intensity

in the camera, compared to the optical axis focused on the center of the two OTR lobes. Given the small acceptance angle of the objective, a large aperture lens could be implemented in the optical line, to gather the OTR onto the camera objective. This unfortunately, has the disadvantage of introducing aberrations to the image, and thus requires additional optics studies before implementation.

A precise cross-alignment of the segmented dump with respect to the aligned OTR screen, using the beam, was not possible during the 2009 run. This was a result of the damaged screen and also because the vacuum window, between the screen and the dump, had a diameter of only 60 mm, which corresponds to roughly 6σ of the transverse beam size. As a consequence, it was not possible to scan the beam over the full screen and the dump, due to the beam interacting with edges of the output vacuum window. Prior to the next PHIN run, the present vacuum window will be replaced with another one of a larger diameter, and thus increasing the acceptance range of the dump. It is foreseen in the next run, to scan the beam in small steps of the dipole current, to fully characterize each dump channel, and also the uniformity of the screens response.

Lastly, during the next PHIN run an attempt to obtain a time resolved measurement of the energy of the beam using the OTR screen will also be made. This can be done by changing the gate of the intensified camera. Therefore scanning a constant integration window across the pulse train given that the beam is stable from shot to shot. The result will then be crosschecked with the segmented dump.

6 Acknowledgments

We would like to thank S. Doebert for his general advice during this study; O. Mete for the beam dynamics simulations and discussions; E. Rugo for the mechanical construction of the segmented dump; C. Dutriat for advice and electrical analysis; S. Burger for calibrating the OTR screens; J. Herranz Alvarez for mechanical advice for the segmented dump; T. Pieloni and L. Rivkin for their support; E. Bravin and M. Olvegaard for useful discussions and E. Chevally for logistics and useful discussions. We would like to finally thank all the PHIN team for the beams, support and help.

References

- [1] G. Bienvenu, *et. al*, “CTF3 3 GHz RF gun test at CERN”, CTF3 Note 093
- [2] R. Roux, “Conception of Photo-injectors for the CTF3 Experiment”, International Journal of Modern Physics A, Volume 22, Issue 22, pp. 3925-3941 (2007)
- [3] K. Honkavaara, “Optical Transition Radiation in High Energy Electron Beam Diagnostics”, Helsinki Institute of Physics, Internal Report, HIP-1999-04
- [4] O. Mete, *et. al*, “Transverse and Longitudinal Beam Characteristics of PHIN Photo Injector at CERN”, Proceedings of DIPAC09, Basel, Switzerland
- [5] D. Egger, “Time resolved energy measurements at PHIN”, CLIC Meeting, July 17 2009

- [6] S. Agostinelli, *et. al.*, “G4 A Simulation Toolkit”, Nuclear Instruments and Methods in Physics Research Section A: Accelerators, Spectrometers, Detectors and Associated Equipment, Volume 506, Issue 3, 1 July 2003, Pages 250-303
- [7] Private communication with O. Mete
- [8] E. Bravin, “*Statistical effects in beam profile monitors*”, AB-Note-2004-016 BDI
- [9] D. Cornuet, G. Patron, “Mesure magnetique du spectrometre 90 K. BHZ 240 du CTF”, AT/MA Note 91-15, PS/LP Note 91-24, Mai 1991

A Appendix

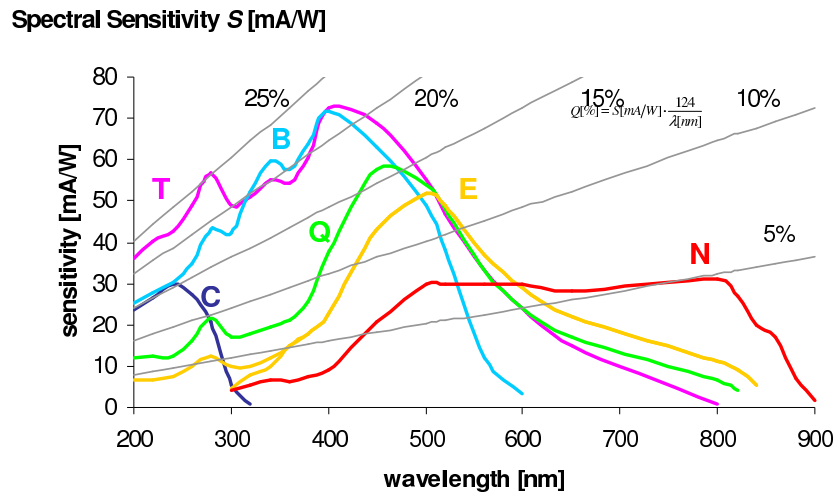


Figure 15: Spectral sensitivity of the cathodes of the Proxitronic intensified cameras. The purple curve corresponds to the camera used in the PHIN spectrometer (T type photocathode).